

# Chemistry in 1d via DMRG: Benchmarks for small atoms, ions, and molecules

Lucas O. Wagner, E.M. Stoudenmire, Kieron Burke,\* and Steven R. White

*Department of Physics and Astronomy, University of California, Irvine, CA 92697*

(Dated: February 23, 2012)

The density matrix renormalization group (DMRG) method, an efficient solver of lattice models in 1d, has been adapted to solve real-space problems. We use DMRG to study the behavior of soft-Coulomb interacting matter, reporting accurate benchmarks for small systems. We compare with Hartree-Fock and the local density approximation, noting similarities and differences with 3d. We study how correlation grows as bonds stretch.

PACS numbers: 71.15.Mb, 31.15.E-, 05.10.Cc

## I. INTRODUCTION AND PHILOSOPHY

Electronic structure methods such as density functional theory (DFT) are excellent tools for investigating the properties of solids and molecules—except when they are not. Standard density functional approximations in the Kohn–Sham (KS) framework [1] work well in the weakly correlated regime [2–4], but these same approximations can fail miserably when the electrons become strongly correlated [5]. Though DFT is exact in principle, what can these successes and failures tell us about the fundamental nature of KS-DFT? In particular, do these failures indicate that approximate KS-DFT cannot describe strongly correlated systems?

Strongly correlated electrons are usually studied with lattice Hamiltonians, which directly model electron localization and spin interactions. Both are correlation effects arising from an underlying continuum model but which are not readily apparent—nor easy to treat—within most methods applicable to real space. As simplified models of bulk materials, lattice Hamiltonians offer qualitative insight into generic behavior, such as phase transitions and collective states of matter. They are often sufficient for extracting universal features, such as scaling exponents near phase transitions, but do not yield highly accurate estimates of material-specific properties, such as bond lengths and atomization energies. Among many clever methods for solving lattice models, DMRG (density-matrix renormalization group) is outstanding for its accuracy and speed, especially for one-dimensional problems, and has been applied to highly-entangled systems with hundreds of lattice sites [6, 7].

An intriguing approach to the problem of strong correlation has been the development of density functional approximations for lattice models. A DFT for lattice models, sometimes called site-occupation functional theory (SOFT), can be formulated and applied to these problems [8]. The most basic energy functional, the local density approximation (LDA), can be found from certain limits solvable by the Bethe ansatz [9]. SOFT approxi-

mations for more exotic quantities such as the entanglement entropy have been tested [10, 11], and exact time-dependent Kohn–Sham DFT has been investigated [12]. Progress in this area provides new approximate methods for solving lattice models at a fraction of the cost of traditional many-body approaches, but with all the usual uncertainties associated with approximate DFT calculations. The main use of such calculations is really as a test of functional ideas on systems (albeit idealized) that have strong correlation.

However, simplified lattice models are *not* good mimics of realistic systems for the properties that are extracted from typical DFT calculations. Take for example a two-site Hubbard model of the hydrogen molecule. Using a minimal basis of a 1s orbital on each H atom, this model becomes relatively exact as the separation tends to infinity, and recovers the Heitler–London wavefunction. Near equilibrium separations, this model becomes empirical, as the parameters are not uniquely determined.

The two-site Hubbard model also highlights a critical difference between the nature of DFT approximations and SOFT approximations. For this model, the SOFT energy functional becomes a function of two numbers (the site occupations) whose sum is constrained by the total particle number. Thus it becomes a simple function. Yet most of the subtleties (and excitements) of DFT *approximations* are because the Hilbert space is infinite, and we use functionals, not functions. Theorems can be proven on lattices that are not true for the exact continuum functionals [13]. Many of the challenges of modern functional approximations concern the delocalization error [14] (a special case of which is self-interaction error [15]). The nature of this error is completely masked when entire atoms are described by single sites. Furthermore, we can rationalize the success of density functional approximations by considering a certain, physically-important scaling of the coordinates: in the semiclassical limit of all continuum systems, LDA becomes exact [16, 17]. This limit can never be attained by a site model with finite-range interactions. It appears that, for SOFT approximations to succeed, they must do so for fundamentally different reasons than real-space DFT approximations.

The work described here is a crucial step toward an entirely new approach to the pressing problem of dealing with strong correlation, with an eye toward bulk materi-

\* Also at Department of Chemistry, University of California, Irvine, CA 92697

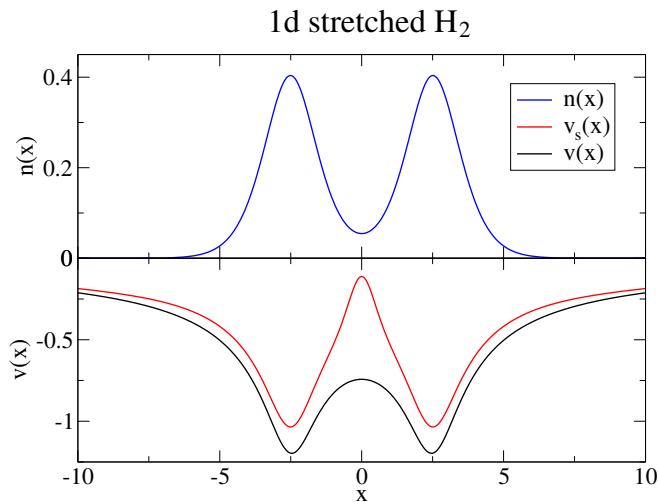


FIG. 1. The KS potential for a stretched hydrogen molecule found from interacting electrons in 1d.

als. Instead of attempting to learn about functionals by defining density functions on lattice models, we adapt an extremely powerful lattice-model solver to work for the continuum. We have built a library of routines that allow application of DMRG to 1d systems with real-space potentials and long-range interactions, instead of lattice models. Compared to past applications of DMRG, this setting far more closely mimics three-dimensional reality, and especially those aspects that are captured by present popular DFT approximations, i.e., the semiclassical limit. In the present work, we present accurate benchmark calculations for small systems, both approximate and exact. These establish the qualitative similarities and differences between this 1d world and the 3d world, and demonstrate how basic questions concerning the performance of density functionals can be directly addressed with this method.

Our results are illustrated in Fig. 1, which shows 1d  $H_2$  with soft-Coulomb interactions. The exact density was found by DMRG and inverted to find the corresponding exact KS potential. The bond has been stretched beyond the Coulson–Fischer point, and a strong XC contribution to the KS potential is needed to reproduce the exact density in the bond region [18]. Such calculations have often been performed for few-electron systems in 3d in the past [19, 20], but our method allows exact treatment of much larger systems. In another paper [21], we show how powerful this method is, by solving a chain of 100 1d H atoms, and by performing interacting inversions. All such calculations were previously unthinkable for systems of this size, and unreachable by any other method. We have applied these techniques to perform the first ever Kohn–Sham calculations using the exact XC functional, essentially implementing the exact Levy–Lieb constrained search definition of the functional, which we will present in yet another paper.

## II. BACKGROUND IN DMRG

The density matrix renormalization group (DMRG) is a powerful numerical method for computing essentially exact many-body ground-state wavefunctions [6]. Traditionally, DMRG has been applied to 1d and quasi-2d finite-range lattice models for strongly correlated electrons [7]. DMRG has also been applied to systems in quantum chemistry, where the long-range Coulomb interaction is distinctive. The Hamiltonians which have been studied in this context include the Pariser–Parr–Pople model [22] and the second-quantized form of the Hartree–Fock equations, where lattice sites represent electronic orbitals [23, 24].

DMRG works by truncating the exponentially large basis of the full Hilbert space down to a much smaller one which is nevertheless able to represent the ground-state wavefunction accurately. Such a truncation would be highly inefficient in a real-space, momentum-space, or orbital basis; rather, the most efficient basis consists of the eigenstates of the reduced density matrix computed across bipartitions of the system [6]. A DMRG calculation proceeds back and forth through a 1d system in a sweeping pattern, first optimizing the ground-state in the current basis then computing an improved basis for the next step. By increasing the number of basis states  $m$  that are kept, DMRG can find the wavefunction to arbitrary accuracy.

The computational cost of DMRG scales as  $N_s m^3$  where  $N_s$  is the number of lattice sites. For gapped systems in 1d, the number of states  $m$  required to compute the ground-state to a specified accuracy is independent of system size, allowing DMRG to scale linearly with  $N_s$ . For gapless or critical systems, the  $m$  needed grows logarithmically with system size, making the scaling only slightly worse. The systems considered here have a relatively low total number of electrons such that the number of states  $m$  required is small, often less than 100. This in turn enables us to work with the very large numbers of sites ( $N_s \sim 1000 - 5000$ ) needed to reach the continuum, as described in more detail below.

## III. METHODOLOGY: CHEMISTRY IN 1D

To apply DFT in its natural context—in the continuum—we shall consider a model of soft-Coulomb interacting matter [25–27], where the electron repulsion has the form

$$v_{ee}(u) = \frac{1}{\sqrt{u^2 + 1}}, \quad (1)$$

and the interaction between an electron and a nucleus with charge  $Z$  and location  $X$  is

$$v(x) = -Zv_{ee}(x - X). \quad (2)$$

The soft-Coulomb interaction is chosen to avoid divergences when particles are close to one another, and

has been used to study molecules in intense laser fields [25, 26]. The wavefunctions and densities within this model lack the cusps present in 3d Coulomb systems. However, the challenge presented by the long-range interactions in 3d Coulomb systems remains for these 1d model systems.

Most DMRG implementations for solving 1d systems have been limited to lattice models with finite-range interactions. Yet we would like to study continuum systems with long-range interactions, systems such as those encountered in quantum chemistry. Although DMRG has been applied in quantum chemistry by having lattice sites represent basis functions [23, 24], such an approach requires a basis appropriate to a particular molecule and is not flexible enough to represent an arbitrary real-space system.

Instead, we enable DMRG to operate in the continuum by discretizing over a fine real-space grid. With a lattice spacing of  $a$ , the real-space Hamiltonian for a 1d system becomes in second quantized notation,

$$H = \sum_{j,\sigma} \frac{-1}{2a^2} (c_{j\sigma}^\dagger c_{j+1,\sigma} + c_{j+1,\sigma}^\dagger c_{j\sigma}) - \tilde{\mu} n_{j\sigma} + \sum_j v^j n_j + \frac{1}{2} \sum_{ij} v_{ee}^{ij} n_i (n_j - \delta_{ij}), \quad (3)$$

where  $\tilde{\mu} = \mu - 1/a^2$ ,  $v^j = v(ja)$  and  $v_{ee}^{ij} = v_{ee}(|i-j|a)$ . The  $\delta_{ij}$  in the last term cancels self interactions. The operator  $c_{j\sigma}^\dagger$  creates (and  $c_{j\sigma}$  annihilates) an electron of spin  $\sigma$  on site  $j$ ,  $n_j = n_{j\uparrow} + n_{j\downarrow}$ , and  $n_{j\sigma} = c_{j\sigma}^\dagger c_{j\sigma}$ . The hopping terms  $c_{j\sigma}^\dagger c_{j+1,\sigma}$  (and complex conjugate) come about from a finite-difference approximation to the second derivative. Like the second-quantized Hamiltonians considered in quantum chemistry, this Hamiltonian corresponds to an extended Hubbard model; Eq. (3), however, is motivated from a desire to study the 1d continuum alongside familiar DFT approximations. Because we require that the potentials and interactions vary slowly on the scale of the grid spacing, the low-energy eigenstates of the discrete Hamiltonian (3) will approximate the continuum system to very high accuracy. Moreover, we check convergence with respect to lattice spacing. Because our potentials—and thus our ground-state densities—vary slowly on the scale of the grid spacing, we can accelerate convergence by using a higher-order finite-difference approximation to the kinetic energy operator; this simply amounts to including more hopping terms in Eq. (3).

Even in its discretized form the Hamiltonian Eq. (3) represents a challenge for DMRG because of the long-range interactions. Including all  $N_s^2$  interaction terms, where  $N_s$  is the number of lattice sites, would make the calculation time scale as  $N_s^3$  overall. Fortunately, an elegant solution has been recently developed [28] which involves rewriting the Hamiltonian as a matrix product operator (MPO)—a string of operator-valued matrices. This form of the Hamiltonian is very convenient

$a$	$c = 8$	$c = 9$	$c = 10$	$c \rightarrow \infty$
0.1000	-81.50	-82.30	-82.40	-82.41
0.0500	-19.58	-20.46	-20.57	-20.58
0.0200	-2.22	-3.16	-3.27	-3.29
0.0100	0.27	-0.68	-0.80	-0.82
0.0050	0.90	-0.07	-0.18	-0.20
0.0025	1.06	0.09	-0.03	-0.05
$\rightarrow 0$	1.12	0.14	0.02	0.00

TABLE I. Convergence of model hydrogen energy with respect to lattice spacing  $a$  and distance  $c$  from the atom to the edge of the system, with differences in units of microhartree from the infinite continuum extrapolation of  $E = -0.66977714$ .

for DMRG, and MPOs naturally encode exponentially-decaying long-range interactions [29]. Assuming that our interaction  $v_{ee}(u)$  can be approximated by a sum of exponentials, the calculation time scales only linearly with the number of exponents  $N_{\text{exp}}$  used. This reduces the computational cost from  $N_s^3$  to  $N_s N_{\text{exp}}$ . In practice, for our soft-Coulomb interactions and modest system sizes ( $N_s < 1000$ ), we find that only  $N_{\text{exp}} = 20$  exponentials are needed to obtain an accuracy of  $10^{-5}$  in our approximate  $v_{ee}(u)$ . The largest  $N_{\text{exp}}$  we use in this paper is 60, which is necessary to find the equilibrium bond length of 1d H<sub>2</sub> accurate to  $\pm 0.01$  bohr (a system with  $N_s \approx 2000$ ).

For technical reasons, we take all of our systems to have open (or box) boundary conditions. This has no adverse effect on our results because we can extend the grid well past our edge atoms. The extra grid sites cost almost no extra simulation time due to the very low density of electrons in the edge regions. To evaluate the dependence of the energy on these edge effects and the grid size, consider Table I. This table shows the convergence of the 1d model hydrogen atom ground-state energy with respect to the lattice spacing  $a$  and the distance  $c$  from the atom to the edge of the system, using the second-order finite difference approximation for the kinetic energy, as in Eq. (3). Our best estimate for the 1d H atom energy is  $-0.66977714$ , converged to at least microhartree accuracy, which differs slightly from that of Eberly [25].

In addition to the accurate many-body solutions offered by DMRG, we can also look at approximate solutions given by standard quantum chemistry tools. Hartree-Fock (HF) theory can be formulated for these 1d systems by trivially changing out the Coulomb interaction for the soft-Coulomb. The exchange energy is then:

$$E_x = -\frac{1}{2} \sum_{\sigma} \sum_{i,j=1}^{N_{\sigma}} \int dx \int dx' v_{ee}(x-x') \times \phi_{i\sigma}(x) \phi_{j\sigma}(x) \phi_{j\sigma}(x') \phi_{i\sigma}(x'). \quad (4)$$

In performing HF calculations, instead of using an orbital basis of Gaussians or some other set of functions, our “basis set” will be the grid, as in Eq. (3). This simple and brute force approach allows us a great degree of flexibility, but is only computationally tractable in 1d.

In this setting we also implement DFT. As mentioned in the introduction, DFT has been applied directly to lattice models. But our model and interaction are meant to mimic the usual application of DFT to the continuum. In particular, the LDA functionals we will use are similar to their 3d counterparts, unlike the Bethe ansatz LDA (BALDA), which has a gap built in [9]. One calculates the LDA exchange energy by taking the exchange energy density per electron for a uniform gas of density  $n$ , namely  $\epsilon_x^{\text{unif}}(n)$ , and then integrating it along with the electronic density:

$$E_x^{\text{LDA}}[n] = \int dx n(x) \epsilon_x^{\text{unif}}(n(x)). \quad (5)$$

We find  $\epsilon_x^{\text{unif}}(n)$  by evaluating Eq. (4) with the KS orbitals of a uniform gas. For a uniform gas, the KS orbitals are the eigenfunctions of a particle in a box, whose edges are pushed to infinity while the bulk density is kept fixed. Because the interaction has a length-scale, i.e.  $v_{ee}(\gamma u) \neq \gamma^p v_{ee}(u)$  for some  $p$ , even exchange is not a simple function. One finds:

$$\epsilon_x^{\text{unif}}(n) = -n f(k_F)/2, \quad (6)$$

where  $k_F = \pi n/2$  is the Fermi wavevector and

$$f(z) = \int_0^\infty dy \frac{\sin^2 y}{y^2} \frac{1}{\sqrt{z^2 + y^2}}. \quad (7)$$

In fact,  $f$  is related to the Meijer  $G$  function [30]:

$$f(z) = G_{2,4}^{2,2} \left( \frac{1}{2}, \frac{1}{2}, 1 \mid \frac{1}{2}, -\frac{1}{2}, 0 \mid z^2 \right) / (4z). \quad (8)$$

We write  $r_s = 1/(2n)$  as the average spacing between electrons in 1d. In Fig. 2, we show the exchange energy per electron for the unpolarized gas as a function of  $r_s$ . For small  $r_s$  (high density),  $\epsilon_x^{\text{unif}} \rightarrow -1/2 + 0.203 r_s$ ; for large  $r_s$  (low density),  $\epsilon_x^{\text{unif}} \rightarrow -0.291/r_s - \ln(r_s)/(4r_s)$ . For contrast, in 3d, the exchange energy per electron is always  $-0.458/r_s$  [31], where  $r_s = (3/(4\pi n))^{1/3}$ .

In practice, we do not use pure DFT, but rather spin-DFT, in which all quantities are considered functionals of the up and down spin densities. In that case, we need LSD, the local spin-density approximation. For exchange, there is a simple spin scaling relation that tells us [32]

$$\epsilon_x^{\text{unif}}(n_\uparrow, n_\downarrow) = -n \sum_{\sigma=\pm 1} (1 + \sigma\zeta)^2 f(k_F(1 + \sigma\zeta))/4, \quad (9)$$

where  $\zeta = (n_\uparrow - n_\downarrow)/n$  is the polarization. This is less trivial than for simple Coulomb repulsion. At high densities, there is no increase in exchange energy due to spin polarization, while there is a huge increase (tending to a factor of 2) at low density, as shown by the solid black line in Fig. 2. In fact,  $\epsilon_x^{\text{unif}}(r_s, \zeta = 1) = \epsilon_x^{\text{unif}}(r_s/2, \zeta = 0)$ .

To complete LDA, we need the correlation energy density of the uniform gas at various densities and polarizations. We are very fortunate to be able to make use of

the pioneering work of Ref. [33], which performs just such a QMC calculation and parametrizes the results, yielding accurate values for  $\epsilon_c^{\text{unif}}(r_s, \zeta)$ , which are also plotted for the unpolarized and fully polarized cases in Fig. 2. These curves are not qualitatively similar to the 3d  $\epsilon_{\text{xc}}^{\text{unif}}(r_s, \zeta)$ . For these 1d model systems, the fully polarized electrons almost completely avoid one another at the exchange level, so that correlation barely decreases their energy for any value of  $r_s$ . For unpolarized electrons, the effect of correlation is to make them avoid each other entirely for low densities ( $r_s > 5$ ) and the XC energy per electron becomes independent of polarization. However, for unpolarized electrons at high density, correlation vanishes with  $r_s$ , and exchange dominates, as in the usual 3d case. For moderate  $r_s$  values, the correlation contribution grows with  $r_s$ , as shown by the red dashed line of Fig. 2. To give an idea of what range of  $r_s$  is important, for the hydrogen atom of Fig. 3, 95% of the density has  $r_s(x) = (2n(x))^{-1}$  between 1 and 8.

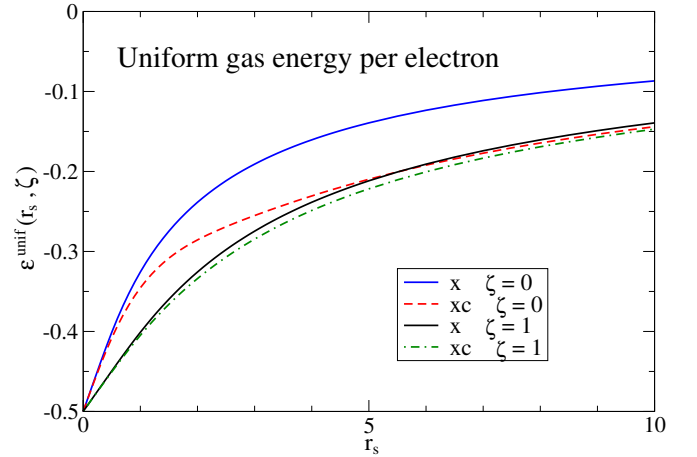


FIG. 2. Parametrization of the LDA exchange and exchange-correlation energy densities per electron for polarized  $\zeta = 1$  and unpolarized  $\zeta = 0$  densities [33].

Armed with these parametrizations and tools, we are ready to discover 1d quantum chemistry.

## IV. RESULTS

DMRG gives us an excellent tool for finding exact answers within a model 1d chemistry world. Our 1d world is designed to mimic qualitatively the 3d world, not match it exactly. Below we explain some important differences between our model 1d systems and real 3d systems, starting with the simplest element.

### A. One-electron atoms and ions

We begin with 1d hydrogen and calculate its ground-state energy to high precision. We find that  $E(H) =$



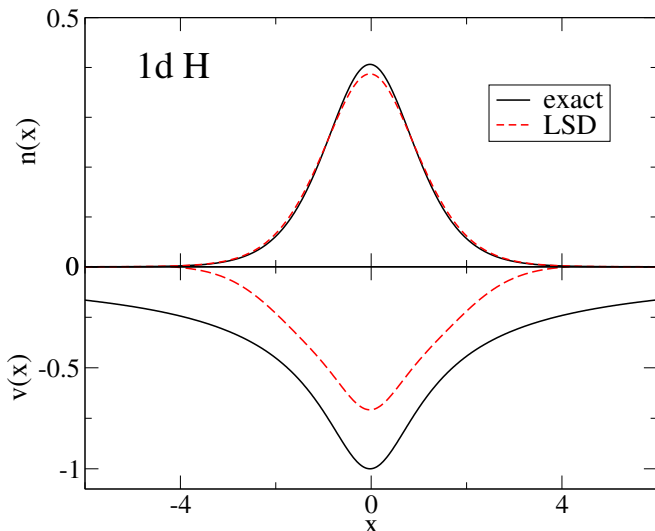


FIG. 3. The hydrogen atom with both exact and LSD densities, as well as the LSD KS potential.

$-0.66977714$ , accurate to 1 microhartree. Table I shows the convergence with respect to the lattice spacing and the size of the system. Eberly et al. [25] were the first to consider the soft-Coulomb hydrogen atom and its eigenstates. Its ground-state energy is similar to the 3d hydrogen atom energy of  $-0.5$  a.u. Because the potential and wavefunction is much smoother, the kinetic energy is only  $0.11$  a.u., as opposed to  $0.5$  a.u. in 3d. Because the potential does not scale homogeneously, in 1d the virial theorem does not yield a simple relation among energy components, unlike 3d.

Again because of the lack of simple scaling, hydrogenic energies do not scale quadratically for our system. A simple fit of energies for  $Z \geq 1$  yields:

$$E_Z \approx -Z + \sqrt{Z}/2 - 2/9 + \alpha_1/\sqrt{Z}, \quad (N=1) \quad (10)$$

where  $\alpha_1 = 0.0524$  is chosen to make the result accurate for  $Z = 1$ . The first two coefficients are exact in the large- $Z$  limit, where the wavefunction is a Gaussian centered on the nucleus.

A well-known deficiency of approximate density functionals is their *self-interaction error*. Because  $E_x$  is approximated, usually in some local or semilocal form, it fails to cancel the Hartree energy for all one-electron systems. Thus, within LSD, the electron incorrectly repels itself. This error can be quantified by looking at how close  $E_x^{\text{LSD}}$  is to the true  $E_x$ . As can be seen in Table II,  $E_x^{\text{LSD}}$  is about 10% too small. For hydrogen, the self-interaction error is about 30 millihartrees. By adding in correlation, this error is slightly reduced, but remains finite. This is an example of the typical cancellation of errors between exchange and correlation in LSD.

As a result of self-interaction error, the LSD electron density spreads out too much, as shown in Fig. 3. In this figure we can also see how the LSD KS potential fails to replicate the true KS potential, which for hydrogen is

system	$T$	$E$	$E^{\text{LSD}}$	$E_x$	$E_x^{\text{LSD}}$	$E_C^{\text{LSD}}$
H	0.111	-0.670	-0.647	-0.346	-0.311	-0.007
He <sup>+</sup>	0.192	-1.483	-1.455	-0.380	-0.343	-0.006
Li <sup>++</sup>	0.258	-2.336	-2.304	-0.397	-0.359	-0.005
Be <sup>+++</sup>	0.316	-3.209	-3.176	-0.408	-0.369	-0.005

TABLE II. Exact and LSD results for 1d one-electron systems.

the same as the external  $v(x)$ . And although the LSD KS potential is almost parallel to  $v(x)$  where there is a large amount of density, it decays too rapidly as  $|x| \rightarrow \infty$ . What this adds up to, both in 1d and in 3d, is that LSD will not bind another electron easily, if at all. We will return to this point when considering anions.

## B. Two-electron atoms and ions

For two or more electrons, the HF approximation is not exact. The traditional quantum chemistry definition of correlation is the error made by HF:

$$E_C^{\text{QC}} = E - E^{\text{HF}}. \quad (11)$$

In Table III, we give accurate energy components for two-electron systems; recall that the components do not satisfy a virial theorem in our 1d systems. The total energy can be fit just as for one-electron systems, but now:

$$E_Z \approx -2Z + \sqrt{Z} + c_0 - \alpha_2/\sqrt{Z}, \quad (N=2) \quad (12)$$

where  $c_0 = 0.507$  and  $\alpha_2 = 0.235$ . The HF energies may be fit with  $c_0^{\text{HF}} = 0.476$  and  $\alpha_2^{\text{HF}} = 0.167$ . These fits are not accurate enough to give the large  $Z$  behavior of  $E_C^{\text{QC}}$ , which seems to vanish as  $Z \rightarrow \infty$ . For 3d two-electron systems, the correlation energy scales to a constant at large  $Z$  [34]. Overall,  $|E_C^{\text{QC}}|$  is much smaller in 1d than in 3d. Rather than the dimensionality, it is the soft nature of our Coulomb interactions that causes the reduction in correlation energy compared to 3d. The exact wavefunctions in 3d have cusps whenever two electrons of opposite spin come together, caused by the divergence of the electron-electron interaction. This cusp-related correlation is sometimes called dynamic correlation; any other correlation, involving larger separations of electrons, is called static [35]. (Note that the distinction between static and dynamic correlation is not precise.) Our soft-Coulomb potential has no divergence and induces no cusps, so dynamical correlation is minimal. There is little static correlation in tightly bound closed shell systems, such as our 1d Li<sup>+</sup> and Be<sup>++</sup>, so  $|E_C^{\text{QC}}| \ll |E|$ . In contrast, for H<sup>-</sup>, where one electron is loosely bound, one expects most of the correlation to be static even in 3d, and one sees large and similar  $E_C$  values in 1d and 3d. In Section IV E, we discuss some quantitative measures of strong correlation.

Next we study the *exact* Kohn–Sham DFT energy components of these two-electron systems. Here we need the

system	$T$	$V$	$V_{ee}$	$E$	$E^{\text{HF}}$	$E_C^{\text{QC}}$
$\text{H}^-$	0.115	-1.326	0.481	-0.731	-0.692	-0.039
He	0.290	-3.219	0.691	-2.238	-2.224	-0.014
$\text{Li}^+$	0.433	-5.084	0.755	-3.896	-3.888	-0.008
$\text{Be}^{++}$	0.556	-6.961	0.790	-5.615	-5.609	-0.006
3d $\text{H}^-$	0.528	-1.367	0.311	-0.528	-0.488	-0.042
3d He	2.904	-6.753	0.946	-2.904	-2.862	-0.042
3d $\text{Li}^+$	7.280	-16.13	1.573	-7.280	-7.236	-0.043
3d $\text{Be}^{++}$	13.66	-29.50	2.191	-13.66	-13.61	-0.044

TABLE III. Exact and HF two-electron atoms and ions, in 1- and 3-d (exact data from Ref. [19],  $\text{Li}^+$  is fit quadratically to surrounding elements, and HF data from Ref. [36, 37]).

	$T_s$	$U$	$E_{xc}$	$E_x$	$E_c$	$T_c$
$\text{H}^-$	0.087	1.103	-0.595	-0.552	-0.043	0.028
He	0.277	1.436	-0.733	-0.718	-0.014	0.013
$\text{Li}^+$	0.425	1.542	-0.779	-0.771	-0.008	0.008
$\text{Be}^{++}$	0.551	1.601	-0.806	-0.801	-0.006	0.005
3d $\text{H}^-$	0.500	0.762	-0.423	-0.381	-0.042	0.028
3d He	2.867	2.049	-1.067	-1.025	-0.042	0.037
3d $\text{Li}^+$	7.238	3.313	-1.699	-1.656	-0.043	0.041
3d $\text{Be}^{++}$	13.61	4.553	-2.321	-2.277	-0.044	0.041

TABLE IV. Energies of the exact KS system for two-electron atoms and ions. 3d data ( $\text{Li}^+$  fitted) from Ref. [19].

DFT definition of correlation, which differs slightly from the traditional quantum chemistry version:

$$\begin{aligned} E_c &= E - (T_s + V + U + E_x) \\ &= T_c + U_c, \end{aligned} \quad (13)$$

where  $E_x$  is the exchange energy of the exact KS orbitals,  $T_s$  is their kinetic energy,  $U$  is the Hartree energy,  $T_c = T - T_s$  is the kinetic correlation energy, and  $U_c = V_{ee} - U - E_x$  is the potential correlation energy. All these functionals are evaluated on the exact ground-state density, with numerical results found in Table IV. The difference between the quantum chemistry  $E_c^{\text{QC}}$  and the DFT  $E_c$  is never negative and typically much smaller than  $|E_c|$  [38]. For the two-electron systems of Table III and Table IV, the difference is zero to the given accuracy for all atoms and ions besides 1d  $\text{H}^-$ . For our systems, just as in 3d,  $E_c^{\text{QC}} - E_c$  vanishes as  $Z \rightarrow \infty$ . All the large DFT components ( $T_s$ ,  $U$ ,  $E_{xc}$ ) are typically smaller than their 3d counterparts and scale much more weakly with  $Z$ . However, our numerical results suggest  $T_c \rightarrow -E_c$  as  $Z \rightarrow \infty$ , just as in 3d.

To obtain the KS energies for a given problem, we require the KS potential, which is found by inverting the KS equation. For one- or two-electron systems, this yields:

$$v_s(x) = \frac{1}{2\sqrt{n(x)}} \frac{d^2}{dx^2} \sqrt{n(x)}. \quad (N \leq 2) \quad (14)$$

For illustration, consider the exact KS potential of 1d helium in Fig. 4. Inverting a density to find the KS potential has also been done for small systems in 3d, where

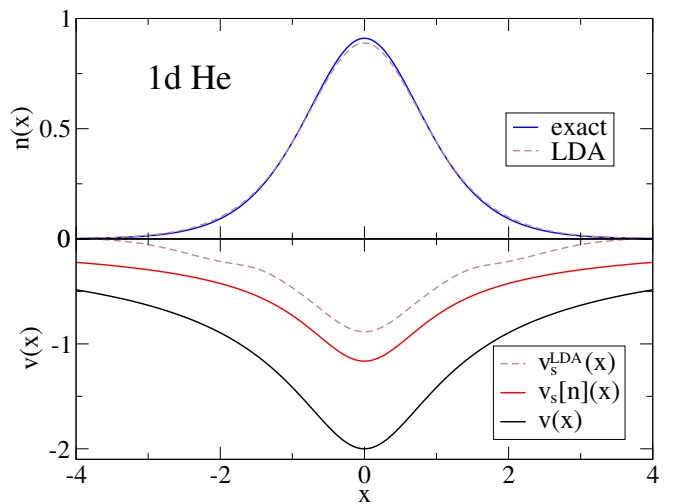


FIG. 4. The exact KS potential for a model helium density found from interacting electrons in 1d, as well as the LDA density and LDA KS potential found self-consistently.

QMC results for a correlated electron density have proven extremely useful [19]. One can find simple and useful constraints on the KS potential by studying the large and small  $r$  behavior of the exact result [19, 39]. In 3d, for large  $r$ , the Hartree potential screens the nuclear potential, and the exchange-correlation potential goes like  $-1/r$  [40]. In 1d, the softness of the Coulomb potential is irrelevant, so the Hartree potential screens the nuclear potential for large  $|x|$  as in 3d. Though it seems likely, we have no proof that the exchange-correlation potential for the soft-Coulomb interaction should tend to  $-1/|x|$  for large  $|x|$ , analogous to the 3d Coulomb result. To check this would require extreme numerical precision in the density far from the atom, due to the need to evaluate Eq. (14) where the density is exponentially small. Instead, in Figures 1 and 4, we require the KS potential to go as  $-b/|x|$  once the density becomes too small (around  $n \approx 10^{-5}$ , which happens at  $|x| \approx 6$  for helium), and we fit  $b$  based on what the potential (14) is doing before that point. The actual value of  $b$  has no visible effect on the density on the scale of these figures.

We now consider the performance of LDA for these two-electron systems, starting with how well LDA replicates the true KS potential. Though the LDA density is only slightly different from the exact density on the scale of Fig. 4, the LDA potential clearly decays too rapidly (exponentially) at large  $r$  and is too shallow overall, just as in 3d [19]. Like the hydrogen atom discussed earlier, this is a result of self-interaction error. LDA energy results are given in Table V. Clearly LDA becomes relatively more accurate as  $Z$  grows, because XC becomes an ever smaller fraction of the total energy. Comparing Tables IV and V, we also see that LDA underestimates the true X contribution by about 5%, while overestimating the correlation contribution, so that XC itself has lower error than either, i.e., a cancellation of errors.

	$E^{\text{LDA}}$	% error	$E_{\text{xc}}^{\text{LDA}}$	$E_{\text{x}}^{\text{LDA}}$	$E_{\text{c}}^{\text{LDA}}$
$\text{H}^-$	-0.708	-3.1%	-0.601	-0.536	-0.065
He	-2.201	-1.7%	-0.690	-0.646	-0.044
$\text{Li}^+$	-3.850	-1.2%	-0.731	-0.696	-0.035
$\text{Be}^{++}$	-5.564	-0.9%	-0.753	-0.723	-0.030
3d $\text{H}^-$	-0.511	-3.2%	-0.419	-0.345	-0.074
3d He	-2.835	-2.4%	-0.973	-0.862	-0.111
3d $\text{Li}^+$	-7.143	-1.9%	-1.531	-1.396	-0.134
3d $\text{Be}^{++}$	-13.44	-1.2%	-2.082	-1.931	-0.150

TABLE V. LDA for 2 electron systems.  $\text{H}^-$  does not converge in 1d or 3d; the results are taken from using the LDA functional on the HF density [41]. 3d LDA data from Engel’s OEP code [42].

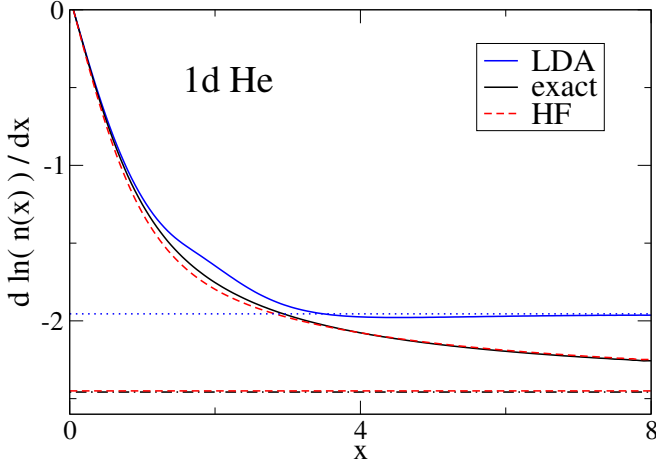


FIG. 5. The differential logarithmic decay of the helium atom density for various methods. The horizontal, dashed lines correspond to the asymptotic decay constants.

Much insight into density functionals has been gained by studying the asymptotic decay of densities and potentials far from the nucleus [39]. In Fig. 5, we plot  $dn/dx/n$  to emphasize the asymptotic decay of the exact, LDA, and HF helium densities. The HF density is very accurate compared to the LDA density. For large  $x$ , the HF density has very nearly the same behavior as the exact density, and both approach their asymptotes very slowly. By contrast, the LDA density reaches its asymptote by  $x \approx 4$ . For each approximate calculation, its asymptotic decay constant  $\gamma$  can be found using the highest occupied molecular orbital (HOMO) energy:  $\gamma = -2\sqrt{-2\epsilon_{\text{HOMO}}}$ . The asymptote for the exact curve can be found using the ionization potential  $I = E(N-1) - E(N)$  of the system, which determines the density decay:  $\gamma = -2\sqrt{2I}$ . Because the HF asymptote lies nearly on top of the exact asymptote, Koopmans’ theorem—or  $I \cong -\epsilon_{\text{HOMO}}^{\text{HF}}$ —is extremely accurate for 1d helium. We list both HOMO and total energy differences in Table VI.

There is a long history of studying two-electron ions in DFT, including the smallest anion  $\text{H}^-$ , which presents interesting conundrums for approximate functionals [43, 44]. Looking at the ionization energies of these 2 electron

system	LSD		HF		exact
	$-\epsilon_{\text{HOMO}}$	$I$	$-\epsilon_{\text{HOMO}}$	$I$	$I = -\epsilon_{\text{HOMO}}$
$\text{H}^-$	—	0.062	0.054	0.022	0.061
He	0.478	0.747	0.750	0.741	0.755
$\text{Li}^+$	1.242	1.546	1.557	1.552	1.560
$\text{Be}^{++}$	2.064	2.389	2.404	2.400	2.406

TABLE VI. 1d HOMO eigenvalues and ionization potentials of two-electron atoms and ions, for the exact functional, LDA, and HF. LDA does not converge for  $\text{H}^-$  anion, but LDA energies can be found using the HF density [41].

systems, we can extrapolate the critical nuclear charge necessary for binding two electrons, i.e., figuring out the  $Z$  value for which  $I = 0$ . This happens around  $Z = 0.90$  in 1d, and around  $Z = 0.91$  in 3d [45]. Within LDA, the critical value is above  $Z = 1$ , because  $\text{H}^-$  will not bind. DFT approximations have a hard time binding anions—both in 1d and in 3d—due to self-interaction error. A way to circumvent this problem is to take the HF anion, which binds an extra electron, and evaluate the LDA functional on its density. As seen in Table VI, this approach is far better than either taking total energy differences or the negative of the HOMO energy from HF alone, just as in 3d [41]. As in 3d,  $-\epsilon_{\text{HOMO}}^{\text{LSD}}$  is useless as an approximation to  $I$ . The HF results  $-\epsilon_{\text{HOMO}}^{\text{HF}}$  and  $I^{\text{HF}}$  are close to each other and closest to  $I$  for larger  $Z$ ; but  $I^{\text{LSD}}$  does very well for small  $Z$ , and is best for  $\text{H}^-$ .

### C. Many-electron atoms

Before looking at larger atoms, a word of caution. In 3d systems, degeneracies in orbitals with different angular momentum quantum numbers produce interesting shell structure. In 1d, there is no angular momentum, and thus a lack of the shell structure we are familiar with. This means that it is not entirely clear which real elements our model 1d atoms correspond to. The first three 1d elements might well be called hydrogen, helium, and lithium; but the fourth 1d element may behave more like neon than beryllium; to be consistent with Ref. [33], we call it beryllium. To showcase 1d Be, consider its LDA treatment in Fig. 6. The exact KS potential is also plotted, and the LDA KS potential roughly differs only by a constant in the high density region, just as with hydrogen (Fig. 3) and helium (Fig. 4). In the low density regions, the LDA correlation potential is the dominant piece of the LDA KS potential.

As we increase the number  $N$  of electrons in our systems, correlation also increases, but HF theory is still better than LDA until  $N = 4$ . Exact and HF data for many-electron atoms can be found in Table VII, and LDA data in Table VIII. Despite good agreement with all other data, we did not find  $\text{He}^-$  or  $\text{Li}^-$  to bind as in Ref. [33], neither in HF nor DMRG, nor LSD (not surprisingly). When using energy differences to calculate the ionization energy, HF outperforms LSD until beryllium, as can be

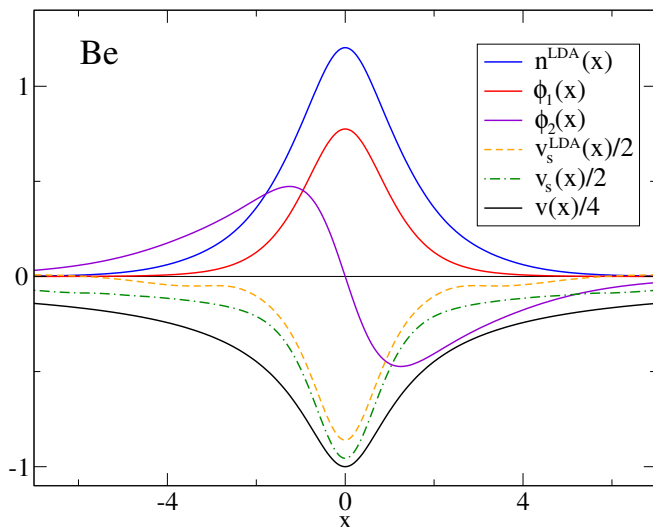


FIG. 6. An LDA “beryllium” atom, complete with the LDA orbitals  $\phi_j(x)$ , LDA KS potential  $v_s^{\text{LDA}}(x)$ , exact KS potential  $v_s(x)$ , and external potential  $v(x)$ . The density  $n^{\text{LDA}}(x)$  was found self-consistently using the LDA method, and barely differs from the true  $n(x)$  on this scale.

system	$T$	$V$	$V_{ee}$	$E$	$E^{\text{HF}}$	$E_C^{\text{QC}}$
Li	0.625	-6.484	1.648	-4.211	-4.196	-0.015
Be <sup>+</sup>	0.922	-9.240	1.864	-6.454	-6.445	-0.010
Be	1.127	-11.13	3.219	-6.785	-6.740	-0.046

TABLE VII. Exact and HF many-electron atoms and ions, in 1d.

seen in Table IX. For these systems,  $I^{\text{LSD}} > I > I^{\text{HF}}$ : LSD overestimates the ionization energy, and HF underestimates it—just as in 3d. As with the fewer electron systems, the LSD HOMO energies are not a good way to estimate  $I$ , whereas the HF HOMO energies are.

	$E^{\text{LSD}}$	% error	$E_{\text{xc}}^{\text{LSD}}$	$E_{\text{x}}^{\text{LSD}}$	$E_{\text{c}}^{\text{LSD}}$
Li	-4.179	-0.8%	-1.044	-1.004	-0.041
Be <sup>+</sup>	-6.410	-0.7%	-1.117	-1.086	-0.031
Be	-6.764	-0.3%	-1.450	-1.376	-0.075

TABLE VIII. LSD energies for many-electron 1d systems.

To find the KS energy components for these many-electron ( $N > 2$ ) systems, we again require the exact KS potential. For these systems, Eq. (14) is no longer valid, so we must find the KS potential another way. The simplest procedure is to use guess-and-check, adjusting the KS potential until its density can no longer be distinguished from the target density found using DMRG. Updates to the KS potential can be more or less sophisticated, without changing the final result in the region where the density is large; in the low-density region, however, two very different KS potentials can give rise to densities that are indistinguishable on the scale of our figures. However, the KS energy components do not rely

system	LSD		HF		exact
	$-\epsilon_{\text{HOMO}}$	$I$	$-\epsilon_{\text{HOMO}}$	$I$	$I = -\epsilon_{\text{HOMO}}$
Li	0.166	0.329	0.316	0.308	0.315
Be <sup>+</sup>	0.628	0.846	0.842	0.835	0.839
Be	0.162	0.353	0.313	0.295	0.331

TABLE IX. Many-electron ionization energies for LSD, HF, and exact 1d systems.

	$T_s$	$U$	$E_{\text{xc}}$	$E_{\text{x}}$	$E_{\text{c}}$	$T_{\text{c}}$
Li	0.611	2.749	-1.087	-1.071	-0.016	0.014
Be <sup>+</sup>	0.912	3.042	-1.168	-1.157	-0.011	0.009
Be	1.091	4.736	-1.481	-1.430	-0.051	0.036

TABLE X. Energies of the exact KS system for many-electron 1d atoms and ions.

significantly on the behavior of the KS potential out in the low-density region. For example, noticeable irregularities occur for the beryllium KS potential, but these occur beyond  $|x| = 7$  and are not plotted in Fig. 6. In Table X, the exact KS energies for some many-electron systems are tabulated. For Li and Be<sup>+</sup>, spin-DFT is used, but the spin-dependent energy components (such as  $T_s^\sigma$ ) are summed together to give a spin-independent energy.

The study of the energies of neutral atoms as  $N = Z \rightarrow \infty$  is important due to the semiclassical result being exact in that limit [16]. In this limit, the oldest of all density functional approximations, Thomas–Fermi (TF) theory, becomes exact [46]. However, due to a lack of scaling within the soft-Coulomb interaction, the large  $Z$  limit of the energy is non-trivial, making a semiclassical treatment difficult. A plot of the neutral atom energies as a function of  $N$  appears in Fig. 7. On this scale, both the LDA and HF results lie nearly on top of the exact curve.

#### D. Equilibrium properties of small molecules

We now briefly discuss small molecules near their equilibrium separation. In order to find the equilibrium bond length for our 1d systems, we take the nuclei to be interacting via the soft-Coulomb interaction, just like the electrons. Given this interaction, consider the simplest of all molecules: the  $\text{H}_2^+$  cation. HF yields the exact answer, and LSD suffers from self-interaction (more generally, a delocalization error [5]). A plot of the binding energy is found in Fig. 8. Because the nuclear-nuclear repulsion is softened, the binding energy does not diverge as the internuclear separation  $R$  goes to zero. As seen in Table XI, LSD overbinds slightly and produces bonds that are too long between H atoms, which is also the case in 3d. The curvature of the LSD binding energy is too small near equilibrium, which makes for inaccurate vibrational energies, especially in 3d. This can also be seen in Table XI. Finally, we note that the energy of stretched  $\text{H}_2^+$  does



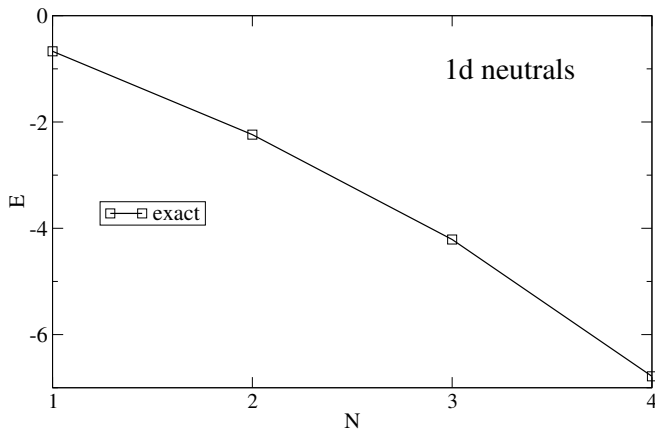
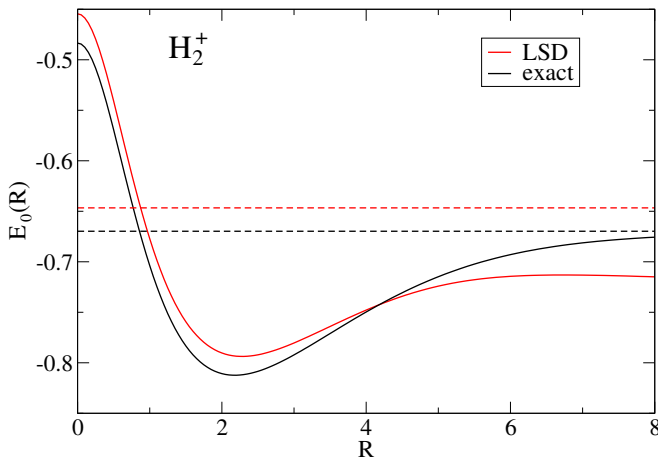


FIG. 7. Energies of neutral atoms in 1d.

FIG. 8. The binding energy curve for our 1d model  $H_2^+$ , shown with an absolute energy scale, and with nuclear separation  $R$ ; horizontal dashed lines indicate the energy of a single H atom.

not tend to that of H within LSD, due to delocalization error [5].

Next we consider  $H_2$ . A plot of the binding energy is found in Fig. 9; the large  $R$  behavior will be discussed in the following section. Just as in 3d, HF underbinds while LDA overbinds; HF bonds are too short, and LDA bonds are too long. Further, HF yields vibrational frequencies which are too high, and LDA are a little small, which is the case both in 1d and 3d. All of these properties can be seen in Table XI.

### E. Quantifying correlation

It is often said that DFT works well for weakly correlated systems, but fails when correlation is too strong. Strong static correlation, which occurs when molecules are pulled apart, is also identified with strong correlation in solids [5]. Functionals that can accurately deal with

	HF	LSD	exact
system	$D_e$ (eV)		
$H_2^+$	3.88 (0%)	4.00 (3%)	3.88
3d $H_2^+$	2.77 (0%)	2.89 (4%)	2.77
$H_2$	2.36 (-23%)	3.53 (15%)	3.07
3d $H_2$	3.54 (-25%)	4.80 (1%)	4.75
system	$R_0$		
$H_2^+$	2.18 (0%)	2.28 (4%)	2.18
3d $H_2^+$	2.00 (0%)	2.18 (9%)	2.00
$H_2$	1.50 (-6%)	1.63 (2%)	1.60
3d $H_2$	1.41 (1%)	1.47 (5%)	1.40
system	$\omega$ ( $\times 10^3$ cm $^{-1}$ )		
$H_2^+$	2.2 (0%)	2.0 (-9%)	2.2
3d $H_2^+$	2.4 (0%)	1.9 (-21%)	2.4
$H_2$	3.3 (6%)	3.0 (-3%)	3.1
3d $H_2$	4.6 (5%)	4.2 (-5%)	4.4

TABLE XI. Electronic well depth  $D_e$ , equilibrium bond radius  $R_0$ , and vibrational frequency  $\omega$  for the  $H_2^+$  and  $H_2$  molecules, with percentage error in parentheses. Exact 3d  $H_2$  results taken from Ref. [47]; the remaining 3d values are from Ref. [36] using the aug-cc-pVDZ basis set [48].

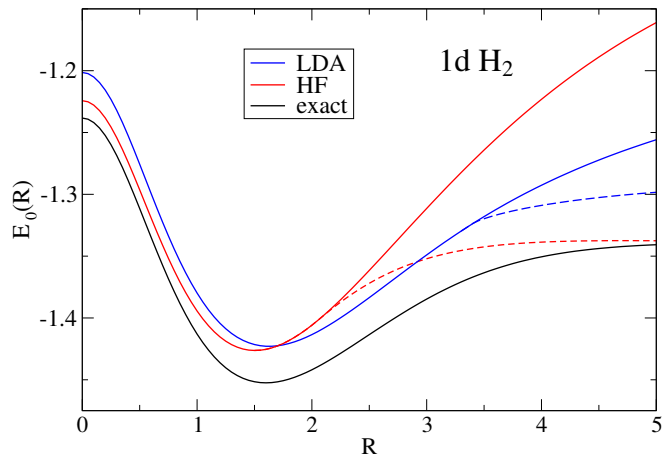


FIG. 9. The binding energy curve for our 1d model  $H_2$ , shown on an absolute energy scale, with nuclear separation  $R$ . Dashed curves represent unrestricted calculations.

strong static correlation in stretched molecules can also accurately yield the band gap of a solid [49, 50]. Most DFT methods, however, fail in these situations. To see these effects in 1d, we shall now examine three descriptors of strong correlation, which will be 0 when no correlation is present and close to 1 when strong correlation is present.

A simple descriptor of strong correlation is simply to calculate the ratio of correlation to exchange:

$$\alpha = \frac{E_C}{E_X}. \quad (15)$$

In the limit of weak electron-electron repulsion,  $\alpha$  goes to zero for closed-shell systems, and HF becomes exact. For example, for the two-electron atoms and ions in Table IV,  $\alpha$  goes to zero as  $Z$  increases. In Table XII, we compute  $\alpha$

for various bond lengths of the hydrogen molecule, both in 1d and in 3d. At the equilibrium bond length,  $\alpha$  is small, indicating that the HF solution is very close to the exact. When the bond is stretched to  $R = 5$ ,  $\alpha$  increases ten-fold: a standard HF solution for a bond length of  $R = 5$  does not do well at all. The 1d and 3d results are remarkably similar. We can also compute  $\alpha$  using the LDA functionals for  $E_C$  and  $E_X$  evaluated on the LDA density; however,  $\alpha^{\text{LDA}}$  is not as good of an indicator for strong correlation as the true  $\alpha$  is.

The second descriptor of strong correlation requires first understanding where correlation comes from. From Eq. (13), correlation can be separated into two pieces: (1) the kinetic correlation energy  $T_C = T - T_s$ , due to the small difference between the true kinetic energy and the KS kinetic energy, and (2) potential correlation energy,  $U_C = V_{ee} - U - E_X$ . In the limit of weak correlation in 3d,  $U_C \rightarrow -2T_C$ , so the ratio:

$$\beta = \frac{E_C + T_C}{E_C} \quad (16)$$

has always been found to be positive, and vanishes in the weakly correlated limit [51], which we have also observed in 1d. But if  $T_C \ll |E_C|$ , we have correlation without the usual kinetic contribution, which occurs when systems have strong *static* correlation. For example, in the infinitely stretched limit of  $\text{H}_2$ ,  $T_s \rightarrow T$  while  $E_C$  remains finite, so  $\beta \rightarrow 1$ . In Table XII, we see that  $\beta$  increases as we stretch the  $\text{H}_2$  molecule, both in 1d and 3d. Thus  $\beta$  is a natural measure of static correlation in chemistry.

There is another test for strong static correlation, which we can use on closed-shell systems. In the absence of a magnetic field, the ground-state wavefunction will be a spin singlet. Yet when stretching a molecule such as  $\text{H}_2$ , there is a bond length beyond which an approximate calculation, such as HF and LDA, will prefer to break spin symmetry in order to lower the energy. This separation is known as the Coulson–Fischer point [52]. Beyond this point, an unrestricted calculation, whose up orbitals may be different than down orbitals, spontaneously breaks spin symmetry. In this case, we say the system has strong static correlation, because the electrons want to localize on different atoms. Before the Coulson–Fischer point, however, both restricted and unrestricted calculations agree, and the system does not have strong static correlation. This phenomenon is observed in Fig. 9, where the solid (dashed) curves repre-

sent restricted (unrestricted) calculations for a stretched hydrogen molecule. Unrestricted HF/LSD breaks spin symmetry around  $R = 2.1/3.4$ , beyond which the unrestricted solution gives accurate total energies, but very incorrect spin densities [53]. The numbers are similar in 3d ( $R = 2.3/3.3$ ) [54].

		1d			3d	
	$R$	1.6	3.4	5.0	1.4	5.0
exact	$\alpha$	0.04	0.21	0.46	0.06	0.45
	$\beta$	0.21	0.58	0.87	0.18	0.89
LDA	$\alpha$	0.09	0.16	0.21		

TABLE XII. Table of correlation descriptors  $\alpha$  and  $\beta$  (Eqs. (15) and (16)) for  $\text{H}_2$  at an equilibrium and a stretched bond length  $R$ . 3d data from Ref. [55].

## V. CONCLUSION

In this paper we have set benchmarks for our 1d model chemistry set. Though this 1d model world is not the same as our 3d world, many properties are similar. Our DMRG results demonstrate that standard approximations like HF and LDA behave just as in the real world. But our approach allows us to study strong correlation that arises directly from the continuum Hamiltonian. Understanding electron correlation in this 1d world will give us insight into real 3d systems, and will illuminate the challenges that we face in making approximate DFT work for strongly correlated systems. Other approaches, such as range-separated hybrids [56], dynamical mean-field theory [57], and LDA+U [58] will be tested in the future.

Using these tools, we seek to develop partition density functional theory (PDFT) [59]. PDFT is a promising method to break up molecules into atoms in a quantitative and exact way. Much like the KS potential, which makes a set of non-interacting electrons look like they are interacting, a new *partition potential* turns non-interacting fragments (such as atoms) into interacting fragments. Hitherto, PDFT has mostly been studied with non-interacting electrons. With the machinery we have developed using DMRG, this will change. Through studying the exact theory, we hope to understand exact and useful constraints on the partition potential and the corresponding partition energy.

With gratefulness, we acknowledge DOE grant DE-FG02-08ER46496 (KB and LW) and NSF grant DMR-0907500 (ES and SW) for supporting this work.

- 
- [1] W. Kohn and L. J. Sham, “Self-consistent equations including exchange and correlation effects,” *Phys. Rev.* **140**, A1133–A1138 (1965).
  - [2] G. Ceder, Y. M. Chiang, D. R. Sadoway, M. K. Aydinol, Y. I. Jang, and B. Huang, “Identification of cathode materials for lithium batteries guided by first-principles calculations,” *Nature* **392**, 694–696 (1998).
  - [3] B. Hammer and J. K. Nørskov, “Theoretical surface science and catalysis - Calculations and concepts,” in *Advances in catalysis, Vol 45: Impact of surface science on catalysis*, Advances in Catalysis, Vol. 45, edited by Gates, B. C. and Knozinger, H. (2000) pp. 71–129.
  - [4] I. J. Casely, J. W. Ziller, M. Fang, F. Furche, and W. J. Evans, “Facile bismuth-oxygen bond cleavage, c-h activa-

- tion, and formation of a monodentate carbon-bound oxyaryl dianion,  $(\text{C}_6\text{H}_2\text{Bu}_2\text{-3,5-o-4})^{2-}$ ,” *J. Am. Chem. Soc.* **133**, 5244–5247 (2011).
- [5] Aron J. Cohen, Paula Mori-Sanchez, and Weitao Yang, “Insights into current limitations of density functional theory,” *Science* **321**, 792–794 (2008).
  - [6] Steven R. White, “Density matrix formulation for quantum renormalization groups,” *Phys. Rev. Lett.* **69**, 2863 (1992); “Density-matrix algorithms for quantum renormalization groups,” *Phys. Rev. B* **48**, 10345 (1993).
  - [7] U. Schollwöck, “The density-matrix renormalization group,” *Rev. Mod. Phys.* **77**, 259–315 (2005).
  - [8] Gao Xianlong, Marco Polini, M. P. Tosi, Vivaldo L. Campo, Klaus Capelle, and Marcos Rigol, “Bethe ansatz density-functional theory of ultracold repulsive fermions in one-dimensional optical lattices,” *Phys. Rev. B* **73**, 165120 (2006).
  - [9] N. A. Lima, M. F. Silva, L. N. Oliveira, and K. Capelle, “Density functionals not based on the electron gas: Local-density approximation for a luttinger liquid,” *Phys. Rev. Lett.* **90**, 146402 (2003); Vivian V. Franca, Daniel Vieira, and Klaus Capelle, “Analytical parametrization for the ground-state energy of the one-dimensional hubbard model,” [arXiv:1102.5018v1](https://arxiv.org/abs/1102.5018v1).
  - [10] V. V. Franca and K. Capelle, “Entanglement in spatially inhomogeneous many-fermion systems,” *Phys. Rev. Lett.* **100**, 070403 (2008).
  - [11] Vivian V. Franca and Irene D’Amico, “Entanglement from density measurements: Analytical density functional for the entanglement of strongly correlated fermions,” *Phys. Rev. A* **83**, 042311 (2011).
  - [12] Claudio Verdozzi, “Time-dependent density-functional theory and strongly correlated systems: Insight from numerical studies,” *Phys. Rev. Lett.* **101**, 166401 (2008).
  - [13] W. Kohn, “ $v$ -representability and density functional theory,” *Phys. Rev. Lett.* **51**, 1596–1598 (1983).
  - [14] Paula Mori-Sánchez, Aron J. Cohen, and Weitao Yang, “Localization and delocalization errors in density functional theory and implications for band-gap prediction,” *Phys. Rev. Lett.* **100**, 146401 (2008).
  - [15] J. P. Perdew and Alex Zunger, “Self-interaction correction to density-functional approximations for many-electron systems,” *Phys. Rev. B* **23**, 5048–5079 (1981).
  - [16] Peter Elliott, Donghyung Lee, Attila Cangi, and Kieron Burke, “Semiclassical origins of density functionals,” *Phys. Rev. Lett.* **100**, 256406 (2008).
  - [17] Attila Cangi, Donghyung Lee, Peter Elliott, and Kieron Burke, “Leading corrections to local approximations,” *Phys. Rev. B* **81**, 235128 (2010).
  - [18] N. Helbig, I. V. Tokatly, and A. Rubio, “Exact kohn–sham potential of strongly correlated finite systems,” *J. Chem. Phys.* **131**, 224105 (2009).
  - [19] C. J. Umrigar and Xavier Gonze, “Accurate exchange-correlation potentials and total-energy components for the helium isoelectronic series,” *Phys. Rev. A* **50**, 3827–3837 (1994).
  - [20] K. Peirs, D. Van Neck, and M. Waroquier, “Algorithm to derive exact exchange-correlation potentials from correlated densities in atoms,” *Phys. Rev. A* **67**, 012505 (2003).
  - [21] E.M. Stoudenmire, Lucas O. Wagner, Steven R. White, and Kieron Burke, “Exact density functional theory with the density matrix renormalization group,” [arXiv:1107.2394v1](https://arxiv.org/abs/1107.2394v1).
  - [22] G. Fano, F. Ortolani, and L. Ziosi, “The density matrix renormalization group method: Application to the PPP model of a cyclic polyene chain,” *The Journal of Chemical Physics* **108**, 9246–9252 (1998).
  - [23] Steven R. White and Richard L. Martin, “Ab initio quantum chemistry using the density matrix renormalization group,” *J. Chem. Phys.* **110**, 4127 (1999).
  - [24] G. K-L. Chan, J. J. Dorando, D. Ghosh, J. Hachmann, E. Neuscamman, H. Wang, and T. Yanai, “An introduction to the density matrix renormalization group ansatz in quantum chemistry,” *Prog. Theor. Chem. and Phys.* **18**, 49 (2008).
  - [25] J. H. Eberly, Q. Su, and J. Javanainen, “High-order harmonic production in multiphoton ionization,” *J. Opt. Soc. Am. B* **6**, 1289–1298 (1989).
  - [26] M. Thiele, E. K. U. Gross, and S. Kümmel, “Adiabatic approximation in nonperturbative time-dependent density-functional theory,” *Phys. Rev. Lett.* **100**, 153004 (2008).
  - [27] J. P. Coe, V. V. Franca, and I. D’Amico, “Feasibility of approximating spatial and local entanglement in long-range interacting systems using the extended hubbard model,” *EPL (Europhysics Letters)* **93**, 10001 (2011).
  - [28] B. Pirvu, V. Murg, J. I. Cirac, and F. Verstraete, “Matrix product operator representations,” *New J. Phys.* **12**, 025012 (2010).
  - [29] Ian P. McCulloch, “From density-matrix renormalization group to matrix product states,” *J. Stat. Mech.*, P10014 (2007).
  - [30] Information about the Meijer  $G$  function can be found online at <http://mathworld.wolfram.com/MeijerG-Function.html>.
  - [31] P. A. M. Dirac, “Note on exchange phenomena in the Thomas atom,” *Mathematical Proceedings of the Cambridge Philosophical Society* **26**, 376–385 (1930).
  - [32] Carlos Fiolhais, F. Nogueira, and M. Marques, *A Primer in Density Functional Theory* (Springer-Verlag, New York, 2003).
  - [33] N. Helbig, J. I. Fuks, M. Casula, M. J. Verstraete, M. A. L. Marques, I. V. Tokatly, and A. Rubio, “Density functional theory beyond the linear regime: Validating an adiabatic local density approximation,” *Phys. Rev. A* **83**, 032503 (2011).
  - [34] Derek Frydel, William M. Terilla, and Kieron Burke, “Adiabatic connection from accurate wave-function calculations,” *The Journal of Chemical Physics* **112**, 5292–5297 (2000).
  - [35] Joshua W. Hollett and Peter M. W. Gill, “The two faces of static correlation,” *The Journal of Chemical Physics* **134**, 114111 (2011).
  - [36] Russell D. Johnson III, ed., *NIST Computational Chemistry Comparison and Benchmark Database*, release 15b ed., NIST Standard Reference Database Number 101 (2011).
  - [37] Ernest R. Davidson, Stanley A. Hagstrom, Subhas J. Chakravorty, Verena Meiser Umar, and Charlotte Froese Fischer, “Ground-state correlation energies for two- to ten-electron atomic ions,” *Phys. Rev. A* **44**, 7071–7083 (1991).
  - [38] E. K. U. Gross, M. Petersilka, and T. Grabo, “Conventional quantum chemical correlation energy versus density-functional correlation energy,” in *Chemical Applications of Density Functional Theory*, Vol. 629, edited by B. B. Laird, R. B. Ross, and T. Ziegler (American

- Chemical Society, Washington, DC, 1996).
- [39] Mel Levy, John P. Perdew, and Virah Sahn, “Exact differential equation for the density and ionization energy of a many-particle system,” *Phys. Rev. A* **30**, 2745–2748 (1984).
  - [40] C. O. Almbladh and A. C. Pedroza, “Density-functional exchange-correlation potentials and orbital eigenvalues for light atoms,” *Phys. Rev. A* **29**, 2322–2330 (1984).
  - [41] Donghyung Lee and Kieron Burke, “Finding electron affinities with approximate density functionals,” *Molecular Physics* **108**, 2687–2701 (2010).
  - [42] E. Engel and R. M. Dreizler, “From explicit to implicit density functionals,” *Journal of Computational Chemistry* **20**, 31–50 (1999).
  - [43] Herbert B. Shore, J. H. Rose, and E. Zaremba, “Failure of the local exchange approximation in the evaluation of the  $h^-$  ground state,” *Phys. Rev. B* **15**, 2858–2861 (1977).
  - [44] Min-Cheol Kim, Eunji Sim, and Kieron Burke, “Communication: Avoiding unbound anions in density functional calculations,” *The Journal of Chemical Physics* **134**, 171103 (2011).
  - [45] B.H. Bransden and C.J. Joachain, *Physics of Atoms and Molecules*, 2nd ed. (Addison-Wesley, 2003).
  - [46] Elliott H. Lieb, “Thomas-fermi and related theories of atoms and molecules,” *Rev. Mod. Phys.* **53**, 603–641 (1981).
  - [47] W. Kolos and L. Wolniewicz, “Improved theoretical ground-state energy of the hydrogen molecule,” *The Journal of Chemical Physics* **49**, 404–410 (1968).
  - [48] Florian Weigend, Andreas Kohn, and Christof Hattig, “Efficient use of the correlation consistent basis sets in resolution of the identity mp2 calculations,” *The Journal of Chemical Physics* **116**, 3175–3183 (2002).
  - [49] Paula Mori-Sánchez, Aron J. Cohen, and Weitao Yang, “Localization and delocalization errors in density functional theory and implications for band-gap prediction,” *Phys. Rev. Lett.* **100**, 146401 (2008).
  - [50] Xiao Zheng, Aron J. Cohen, Paula Mori-Sánchez, Xi-angqian Hu, and Weitao Yang, “Improving band gap prediction in density functional theory from molecules to solids,” *Phys. Rev. Lett.* **107**, 026403 (2011).
  - [51] Kieron Burke, J.P. Perdew, and Matthias Ernzerhof, “Mixing exact exchange with gga: When to say when,” in *Electronic Density Functional Theory: Recent Progress and New Directions*, edited by J. F. Dobson, G. Vignale, and M. P. Das (Plenum, NY, 1997) p. 57.
  - [52] C.A. Coulson and I. Fischer, “Xxxiv. notes on the molecular orbital treatment of the hydrogen molecule,” *Philosophical Magazine Series 7* **40**, 386–393 (1949).
  - [53] John P. Perdew, Andreas Savin, and Kieron Burke, “Escaping the symmetry dilemma through a pair-density interpretation of spin-density functional theory,” *Phys. Rev. A* **51**, 4531–4541 (1995).
  - [54] Rudiger Bauernschmitt and Reinhart Ahlrichs, “Stability analysis for solutions of the closed shell kohn–sham equation,” *The Journal of Chemical Physics* **104**, 9047–9052 (1996).
  - [55] M. Fuchs, Y.-M. Niquet, X. Gonze, and K. Burke, “Describing static correlation in bond dissociation by kohn–sham density functional theory,” *The Journal of Chemical Physics* **122**, 094116 (2005).
  - [56] A. Savin, in *Recent Developments and Applications of Modern Density Functional Theory* (Elsevier, 1996) pp. 327–357.
  - [57] Antoine Georges, Gabriel Kotliar, Werner Krauth, and Marcelo J. Rozenberg, “Dynamical mean-field theory of strongly correlated fermion systems and the limit of infinite dimensions,” *Rev. Mod. Phys.* **68**, 13–125 (1996).
  - [58] Vladimir I Anisimov, F Aryasetiawan, and A I Liechtenstein, “First-principles calculations of the electronic structure and spectra of strongly correlated systems: the lda + u method,” *Journal of Physics: Condensed Matter* **9**, 767 (1997).
  - [59] Peter Elliott, Kieron Burke, Morrel H. Cohen, and Adam Wasserman, “Partition density-functional theory,” *Phys. Rev. A* **82**, 024501 (2010).